ACS NANO
Cite This: ACS Nano 2019, 13, 8417−8424
www.acsnano.org

ARTICLE

One-Pot, Large-Scale Synthesis of Organic Color Center-Tailored Semiconducting Carbon Nanotubes

Hong-Bin Luo,[†,§,∥] Peng Wang,[†,∥] Xiaojian Wu,[†] Haoran Qu,[†] Xiaoming Ren,[§] and YuHuang Wang*[,†,‡]

[†]Department of Chemistry and Biochemistry, University of Maryland, College Park, Maryland 20742, United States
[‡]Maryland NanoCenter, University of Maryland, College Park, Maryland 20742, United States
[§]State Key Laboratory of Materials-Oriented Chemical Engineering and College of Chemistry and Molecular Engineering, Nanjing Tech University, Nanjing 210009, P. R. China

Supporting Information

ABSTRACT: Organic color center-tailored semiconducting single-walled carbon nanotubes are a rising family of synthetic quantum emitters that display bright defect photoluminescence molecularly tunable for imaging, sensing, and quantum information processing. A major advance in this area would be the development of a high-yield synthetic route that is capable of producing these materials well exceeding the current μg/mL scale. Here, we demonstrate that adding a chlorosulfonic acid solution of raw carbon nanotubes, sodium nitrite, and an aniline derivative into water readily leads to the synthesis of organic color center-tailored nanotubes. This unexpectedly simple one-pot reaction is highly scalable (yielding hundreds of milligrams of materials in a single run), efficient (reaction completes in seconds), and versatile (achieved the synthesis of organic color centers previously unattainable). The implanted organic color centers can be easily tailored by choosing from the more than 40 aniline derivatives that are commercially available, including many fluoroaniline and aminobenzoic acid derivatives, and that are difficult to convert into diazonium salts. We found this chemistry works for all the nanotube chiralities investigated. The synthesized materials are neat solids that can be directly dispersed in either water or an organic solvent by a surfactant or polymer depending on the specific application. The nanotube products can also be further sorted into single chirality-enriched fractions with defect-specific photoluminescence that is tunable over ∼1100 to ∼1550 nm. This one-pot chemistry thus provides a highly scalable synthesis of organic color centers for many potential applications that require large quantities of materials.

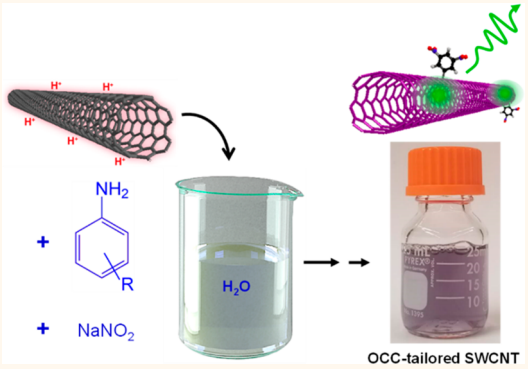

KEYWORDS: *single-walled carbon nanotube, organic color center, photoluminescence, single-defect spectroscopy, shortwave infrared, quantum emitter, sp³ quantum defect*

Organic color centers (OCCs), which are sp^3 quantum defects intentionally implanted into the sp^2 lattice of semiconducting single-walled carbon nanotubes (SWCNTs),[1−11] are being intensively investigated because of their molecularly tunable defect photoluminescence (PL) in the shortwave infrared.[1,2,7−9] The implanted sp^3 defects create local potential wells in the semiconducting SWCNT host, allowing mobile excitons to be harvested at the trapping defect and converted into infrared PL with high efficiency and single-photon purity.[1,7,8,10] These exciting properties have motivated the exploration and demonstration of room temperature quantum light emitters,[8,12] near-infrared (NIR)-II bioimaging contrast agents,[13,14] and *in situ* biological pH sensors.[15] However, the synthesis of OCC-SWCNTs is currently limited at the μg/mL scale, which prevents the exploration of many potential applications that require larger quantities of materials. For example, in the case of bioimaging applications, the *in vivo* administration to small animals (*e.g.*, mice and rats) typically requires SWCNT concentrations ranging from ∼0.1 to 10 mg/kg,[16,17] corresponding to at least milligrams for administration to an adult human. Furthermore, large-scale synthesis is also required to reduce processing costs and minimize batch-to-batch variations.[17]

Received: May 25, 2019
Accepted: July 3, 2019
Published: July 3, 2019

DOI: 10.1021/acsnano.9b04087
ACS Nano 2019, 13, 8417−8424

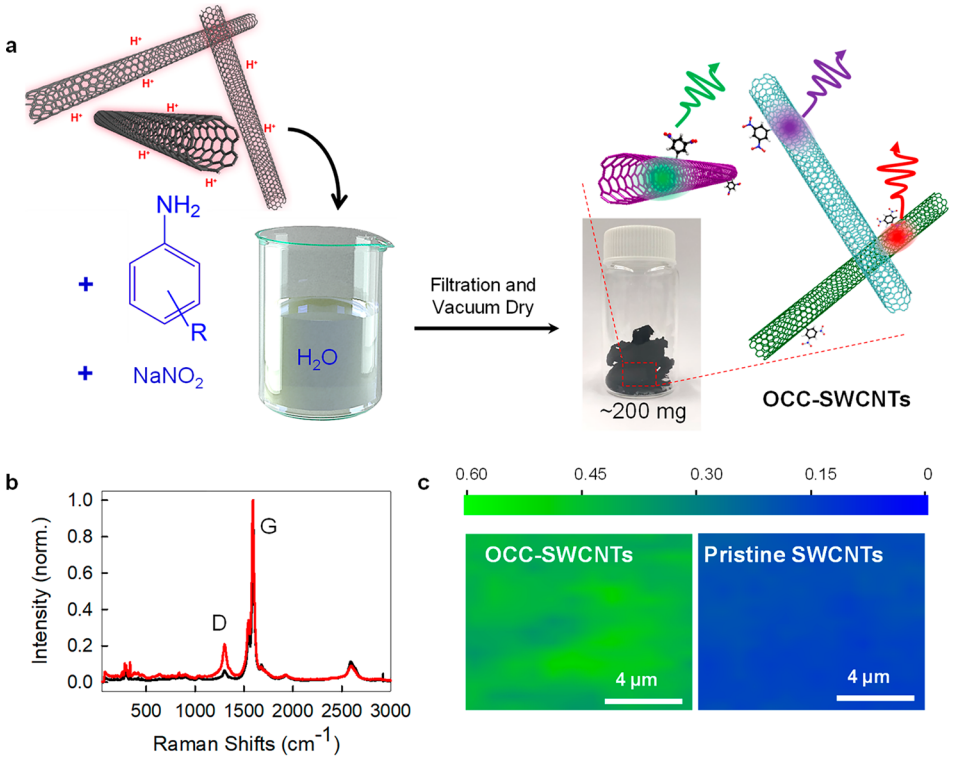

Figure 1. One-pot, large-scale synthesis of OCC-SWCNTs. (a) The reaction occurs by mixing SWCNTs, aniline derivatives, and $NaNO_2$ in chlorosulfonic acid, followed by introducing the mixture into water. (b) Raman scattering from thin films of $C_6H_3(NO_2)_2$-OCC-tailored-SWCNTs (red) and pristine SWCNTs (black), and (c) the spatial maps of the Raman D/G ratios (plotted in color scale). The laser excitation is 633 nm.

The synthesis of OCC-SWCNTs generally involves implanting sp^3 defects onto semiconducting SWCNT surfaces through the formation of C−C covalent bonds. A scalable synthetic route to produce this promising material should thus meet three prerequisites: (1) the ability to process a large amount of SWCNTs as the reactant material; (2) a facile chemistry to create C−C bonds; and (3) a solvent to individually disperse SWCNTs at high concentrations so that the nanotube surfaces are accessible for the OCC-implanting chemistry. The mass production of SWCNTs has been commercially achieved (*e.g.*, up to 10 tons per year scale at OCSiAl), which provides a sufficient source of raw SWCNTs. However, as-synthesized SWCNTs are bundled due to strong van der Waals attractions, making the nanotube surface largely inaccessible to reactant molecules. As a result, individualizing SWCNTs is necessary to increase the efficiency of OCC-implanting chemistry.

Toward this end, previous methods of synthesizing OCC-SWCNTs have involved stabilizing individual SWCNTs by surfactants in aqueous solution as the first step. However, even with the aid of surfactants, the concentration of SWCNTs that are functionalized is still low.[18] Moreover, using surfactants to stabilize individual SWCNTs incurs a serious trade-off: strong surfactants, such as sodium deoxycholate (DOC), effectively stabilize SWCNTs by homogeneously and tightly encapsulating the nanotubes, which in turn makes the nanotube surface less accessible for subsequent reactions.[19,20] Alternatively, weaker surfactants, like sodium dodecyl sulfate (SDS), form loose and disordered micelle structures that only partially cover the nanotube side walls.[20,21] Although the uncovered regions are reactive to subsequent OCC implantations, SDS-stabilized SWCNTs rebundle more easily. Additionally, the highest concentration of SDS-stabilized SWCNTs is only ∼18 μg/mL,[22] making it difficult to scale up the chemical reaction.

Here, we demonstrate a one-pot synthesis of OCC-SWCNTs capable of producing at the hundreds of milligrams scale at high concentrations (>4000 μg/mL) by an efficient reaction process that completes in seconds. This one-pot reaction involves simply mixing raw SWCNTs, an aniline derivative, and $NaNO_2$ in chlorosulfonic acid and then adding the mixture into nanopure water. We further show that the OCC-SWCNTs can be directly sorted into single-chirality enriched OCC-SWCNTs featuring characteristic defect PL.

RESULTS AND DISCUSSION

Figure 1a schematically describes this one-pot synthesis of OCC-SWCNTs. As a demonstration of this synthetic approach, we mixed raw nanotube powders (CoMoCAT SG 65i), $NaNO_2$, and 3,5-dinitroaniline in chlorosulfonic acid and then slowly added the mixture into nanopure water. This resulted in the synthesis of OCC-SWCNTs, mainly 3,5-dinitroaryl-OCC tailored-(6,5)-SWCNTs (hereafter referred as $C_6H_3(NO_2)_2$-OCC-tailored-(6,5)-SWCNT), as black precipitates, which can be collected via vacuum filtration (see Methods for details). We confirmed the covalent modification to the sp^2 carbon lattice by Raman spectroscopy, which reveals a significant increase of the D/G ratio (the intensity of the D peak at ∼1300 cm^{-1} to the G peak at ∼1600 cm^{-1}) to ∼0.5, compared with ∼0.1 for the starting raw SWCNTs (Figure 1b,c). This one-pot reaction allows us to synthesize OCC-SWCNTs at the hundreds of milligrams scale in a straightforward manner. Figure 1a shows a batch of $C_6H_3(NO_2)_2$-OCC-tailored-SWCNTs weighing ∼200 mg.

DOI: 10.1021/acsnano.9b04087
ACS Nano 2019, 13, 8417−8424

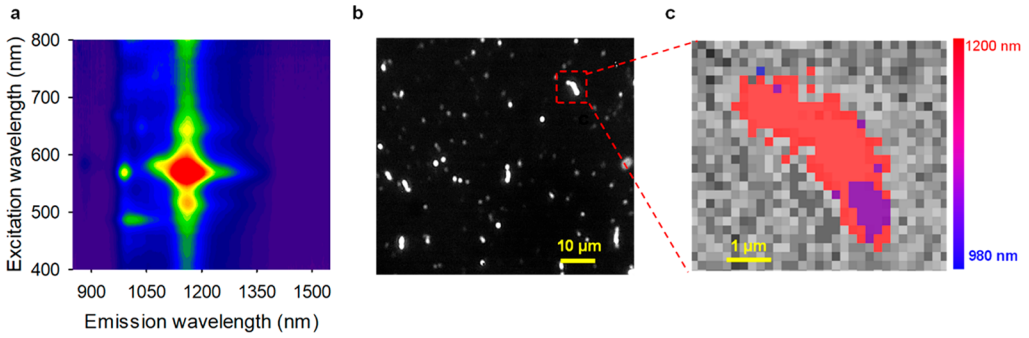

Figure 2. $C_6H_3(NO_2)_2$-OCC-tailored-SWCNTs fluoresce brightly in the shortwave infrared. (a) PL excitation−emission map of $C_6H_3(NO_2)_2$-OCC-tailored-SWCNTs in 2% (w/v) DOC-D_2O solution. (b) Single particle PL imaging of $C_6H_3(NO_2)_2$-OCC-tailored-SWCNTs. (c) Hyperspectral PL image of an individual $C_6H_3(NO_2)_2$-OCC-tailored-(6,5)-SWCNT.

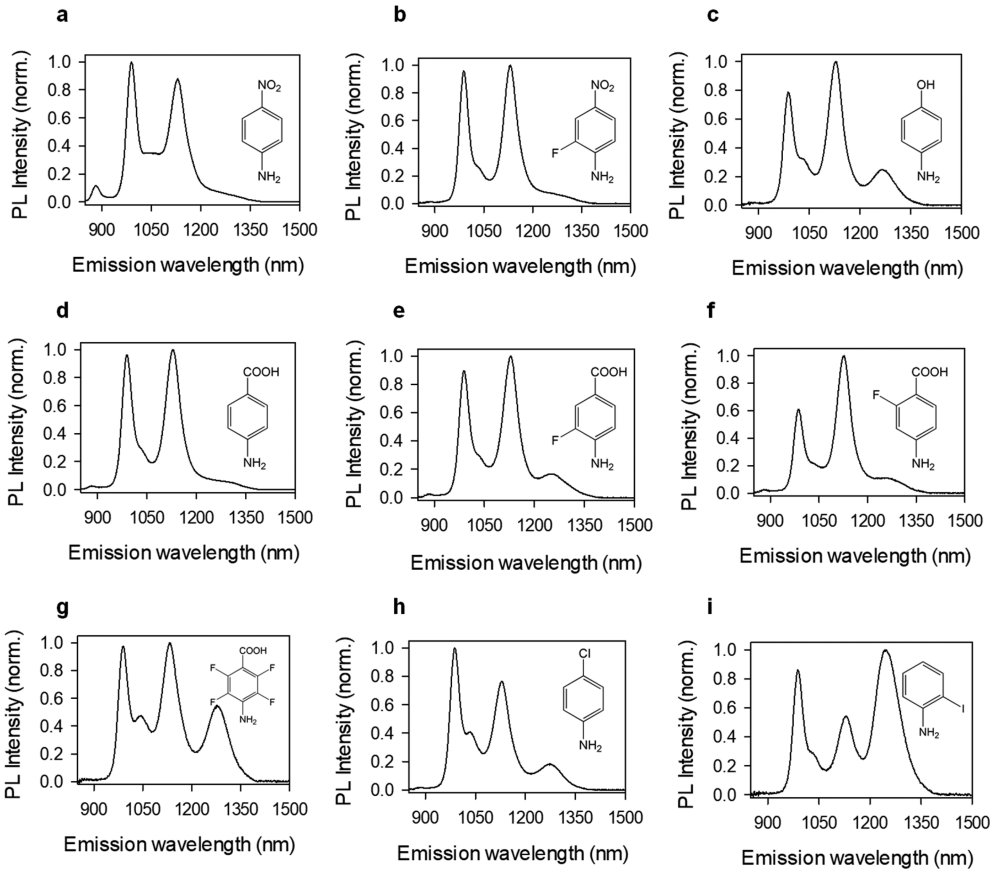

Figure 3. PL spectra (at 565 nm excitation) of OCC-SWCNTs tailored with a wide variety of aniline OCCs, including (a) 4-nitroaniline, (b) 2-fluoro-4-nitroaniline, (c) 4-aminophenol, (d) 4-aminobenzoic acid, (e) 4-amino-2-fluorobenzoic acid, (f) 4-amino-3-fluorobenzoic acid, (g) 4-amino-2,3,5,6-tetrafluorobenzoic acid, (h) 4-chloroaniline, and (i) 2-iodoaniline. The OCC-SWCNTs were stabilized as individual particles in 2% (w/v) DOC-D_2O solution. We note that 2-fluoro-4-nitro-aryl (b), 4-amino-2-fluorobenzoic acid (e), and 4-amino-2,3,5,6-tetrafluorobenzoic acid (g) OCCs were synthetically achieved by this one-pot reaction.

To characterize the photoluminescence properties, we dispersed the synthesized $C_6H_3(NO_2)_2$-OCC-tailored-SWCNT material in 2% (w/v) DOC-D_2O and measured the excitation−emission map (Figure 2a). A bright defect PL (E_{11}^-) was observed at ∼1160 nm, which is red-shifted by 170 nm (184 meV) from the native E_{11} emission of pristine (6,5)-SWCNTs (Figure S1). This E_{11}^- PL originates from the mobile excitons that are efficiently trapped at the OCC defect sites and emit as photons.[1,7] We note that the OCCs synthesized by this one-pot method exhibit remarkable stability (more than 4 months; Figure S2) and similar high brightness (Figure S3) compared to OCCs created by diazonium reactions in aqueous solution.[1]

We further performed hyperspectral fluorescence imaging using a custom-built microscope[23] to investigate the defect PL at the individual OCC-SWCNT level. Figure 2b shows a broadband (1100−1600 nm) PL image of the $C_6H_3(NO_2)_2$-OCC-tailored-SWCNT sample with a long-pass filter at 1100 nm to filter out the pristine E_{11} PL emission. Hyperspectral imaging was then performed to resolve the spatial distribution of defects along the length of individual OCC-SWCNTs. Figure 2c shows the emission wavelength map of an individual,

DOI: 10.1021/acsnano.9b04087
ACS Nano 2019, 13, 8417−8424

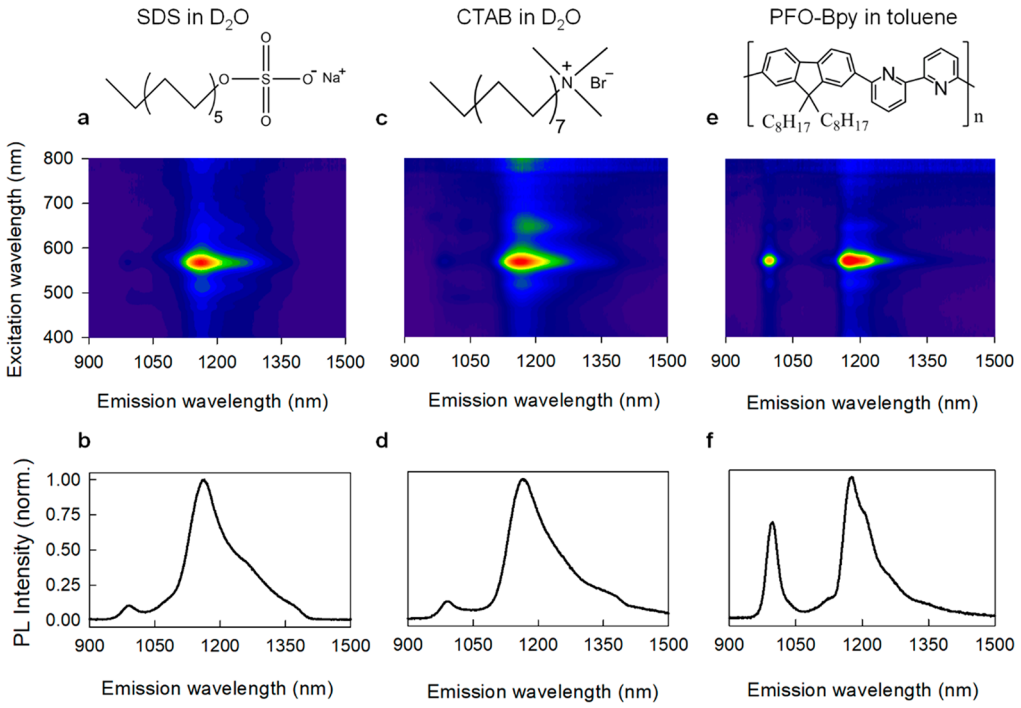

Figure 4. Individual OCC-SWCNTs encapsulated directly by various molecules and polymers. PL excitation−emission maps and spectra (565 nm excitation) of $C_6H_3(NO_2)_2$-OCC-tailored-SWCNTs that are directly dispersed in (a, b) 2% (w/v) SDS, (c, d) CTAB in D_2O, and (e, f) PFO-BPy in toluene.

~4 μm long $C_6H_3(NO_2)_2$-OCC-tailored-(6,5)-SWCNT, which features homogeneous defect E_{11}^- PL emission at ~1160 nm along the entire nanotube axis. This indicates uniform side wall functionalization of the SWCNTs, presumably due to the fact that the SWCNTs dispersed in superacid are bare (*i.e.*, without surfactant),[24] thus exposing the whole surface of the material and making it readily accessible to the reactant molecules. We also note that, by controlling the relative amounts of reactants (3,5-dinitroaniline and SWCNTs), the functionalization degree and resulting PL intensity of $C_6H_3(NO_2)_2$-OCC-tailored-SWCNT can be easily controlled. In Figure S1b, we show that the defect PL intensity of $C_6H_3(NO_2)_2$-OCC-tailored-(6,5)-SWCNT reaches its maximum at a reactant to carbon molar ratio ([aniline]:[C]) of ~1:50 (note that the carbons in this case account for all nanotube chiralities and other carbon species in the starting SG65i raw material). Excessive reaction ultimately quenches the PL of both E_{11} and E_{11}^-.

Because the optical behavior of an OCC is strongly dependent on the chemical nature of the defect,[1,7] the tunability of the functional group is particularly valuable for OCC chemistries. Figure 3 shows the PL spectra of OCC-SWCNTs functionalized by a wide variety of aniline derivatives, including fluoroaniline and aminobenzoic acid derivatives, and some of them (*e.g.*, 2-fluoro-4-nitroaniline, 4-amino-2-fluorobenzoic acid, and 4-amino-2,3,5,6-tetrafluorobenzoic acid (see Figure S4 for the excitation−emission maps)) have never been achieved in aqueous-based reactions due to the difficulty in synthesizing the corresponding diazonium salts,[1,7] demonstrating the versatility of this one-pot chemistry.

We further show that long, individually dispersed OCC-SWCNTs can be directly obtained in a superacid−surfactant exchange (S2E) process[25−27] by simply adding the superacid-SWCNT-reactant mixture into a DOC/NaOH solution. As the superacid is quenched by NaOH, the OCC-SWCNTs are instantly stabilized by the DOC surfactants as individual particles in water. We note that the resulting OCC-SWCNTs obtained directly by this S2E process exhibit much lower E_{11}^- PL emission when compared with that of water-quenched OCC-SWCNTs (Figure S5). This is possibly due to competition between the DOC surfactant and the reactant molecules in coating the exposed SWCNTs as the chlorosulfonic acid leaves. DOC coating of the nanotube surfaces will prevent the further attachment of aniline molecules to the carbon lattice.[19] We addressed this problem by redissolving the water quenched OCC-SWCNTs materials in the superacid and then performed S2E as a separate step (see the Methods for details). In this manner, we were able to obtain long OCC-SWCNTs with an average length of ~1.55 μm (Figure S6) that exhibited much brighter E_{11}^- PL (Figure S7).

In addition to the scalability, another significant advantage of this synthetic route is that OCC-SWCNTs are produced as solid bulk materials, which we hypothesized could be dissolved into a wide spectrum of solvents with different types of surfactants or polymers, depending on the specific requirements of subsequent processing steps necessary for different applications. For instance, in the case of biomedical imaging and therapy, surfactant molecules are typically highly toxic and cause biocompatibility concerns.[28] Also, excess free surfactant molecules that are not physically adsorbed on the SWCNTs are difficult to remove from the solution, creating an obstacle to the further conjugation of SWCNTs with imaging labels or bioactive molecules.[14] Although prolonged dialysis can be used to exchange bioincompatible surfactants (such as SDS) to other biocompatible and stable molecules, the method

DOI: 10.1021/acsnano.9b04087
ACS Nano 2019, 13, 8417−8424

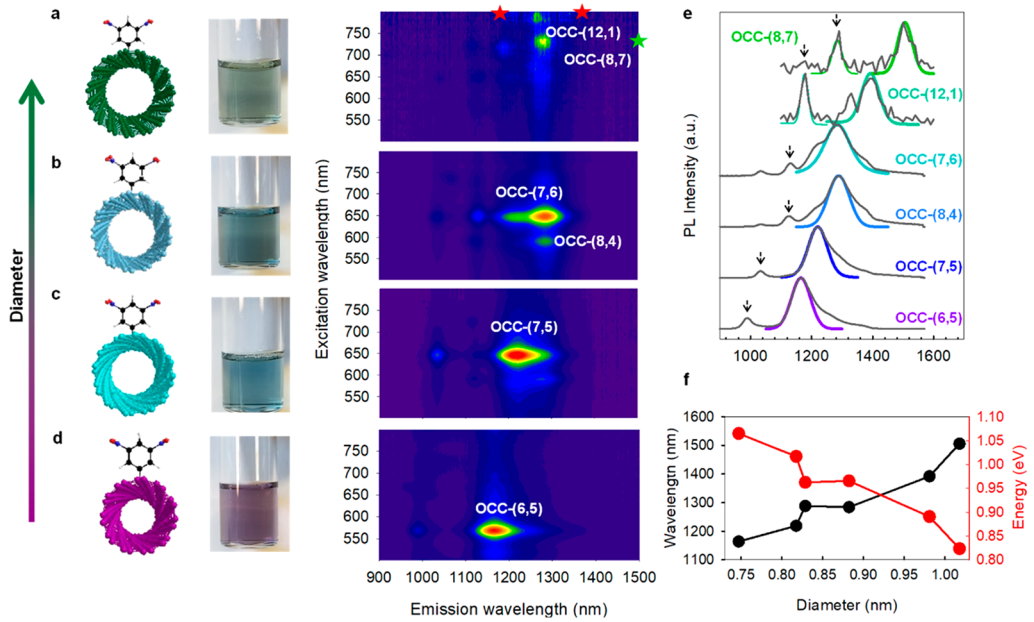

Figure 5. Single chirality-enriched OCC-SWCNTs. DOC-D_2O solutions of (a) (8,7), (b) (7,6), (c) (7,5), and (d) (6,5)-enriched $C_6H_3(NO_2)_2$-OCC-tailored-SWCNTs, along with their corresponding PL excitation−emission maps. Due to the strong water absorption above the wavelength of 1350 nm, the defect PL (E_{11}^-) peak could not be directly detected in the aqueous solutions of $C_6H_3(NO_2)_2$-OCC-tailored-(12,1)-SWCNTs and $C_6H_3(NO_2)_2$-OCC-tailored-(8,7)-SWCNTs. The green and red stars in (a) are the peak positions measured by the hyperspectral imaging of individual nanotubes deposited on a substrate. (e) PL spectra of $C_6H_3(NO_2)_2$-OCC-tailored-SWCNTs made from different chiralities. The spectra were fitted with Voigt functions. The arrows indicate the E_{11} wavelength of $C_6H_3(NO_2)_2$-OCC-tailored-SWCNTs. (f) Correlation of E_{11}^- with the host nanotube diameters for $C_6H_3(NO_2)_2$-OCC-tailored-SWCNTs.

is time-consuming and the recovery yield is usually very low (<30%).[29]

Here, we demonstrate that the resulting OCC-SWCNTs can be stabilized by a wide variety of surfactants and polymers, including SDS, cetrimonium bromide (CTAB) in D_2O, and poly[(9,9-dioctylfluorenyl-2,7-diyl)-*alt*-*co*-(6,6′-{2,2′-bipyridine})] (PFO-BPy) in toluene, all of which exhibit bright defect PL (Figure 4). The relatively low E_{11}^-/E_{11} ratio of the PFO-BPy wrapped OCC-SWCNTs dispersed in toluene can be attributed to the strong optical absorption of the toluene solvent at the wavelengths from 1100 to 1250 nm (Figure S8), which overlaps with the E_{11}^- emission. It is noteworthy that the PFO-BPy wrapped OCC-SWCNTs dispersed in toluene show E_{11}^- emission with a much narrower full width at half-maximum (fwhm) of ∼63 meV compared with those dispersed in aqueous solution (∼96 meV and ∼103 meV for SDS and CTAB, respectively). This is possibly due to the absence of charge transfer from the nanotube OCCs to the nonpolar toluene solvent[30] and may be also affected by the optical absorption from toluene.

Single chirality SWCNTs possess characteristic optical absorption and emission because of their distinct electronic band structure. For single chirality OCC-SWCNTs,[31] the unique optical properties include not only the native PL features of the nanotube host but also the added defect PL, both of which are important to fully exploit the extraordinary PL properties for practical applications in optoelectronics. For example, single chirality OCC-SWCNTs are sought after as high-purity single-photon sources for quantum information processes.[32]

We further show that the synthesized OCC-SWCNTs can be sorted by adopting established nanotube purification techniques such as aqueous two-phase extraction (ATPE).[33−35] Here, we developed an ATPE recipe that allows us to directly sort OCC-SWCNTs to attain single chirality-enriched fractions at large volumes (Figure S9). Figure 5a−d shows four sorted solutions of $C_6H_3(NO_2)_2$-OCC-tailored-SWCNTs, including OCC-(6,5)-SWCNT, OCC-(7,5)-SWCNT, OCC-(7,6)-SWCNT, and OCC-(8,7)-SWCNT. We note that the $C_6H_3(NO_2)_2$-OCC-tailored-(8,7)-SWCNT fraction also contained some OCC-(12,1)-SWCNTs. To avoid the strong water absorption at wavelengths greater than ∼1350 nm, we measured the E_{11}^- peaks of the larger diameter $C_6H_3(NO_2)_2$-OCC-tailored (12,1)-SWCNTs and (8,7)-SWCNTs in the solid state by hyperspectral imaging (Figure S10). We observed that as the diameter of the host nanotube increases, the E_{11}^- emission from the OCCs red-shifted from ∼1160 nm in the smallest (6,5) host to ∼1510 nm in the largest (8,7) host (Figure 5e). This diameter dependence is consistent with previous results[9] and is due to the different depths of exciton traps for hosts of different diameters.[36] The general correlation between E_{11}^- with the host nanotube diameter is further shown in Figure 5f. Notably, the (8,7) chirality is one of the largest diameter (∼1.02 nm) SWCNTs ever reported as a host for OCCs, and the corresponding OCC-SWCNT sample features the most red-shifted defect PL at ∼1510 nm, which falls within the telecommunication range. This result is significant in that SWCNTs with large diameters are difficult to functionalize in aqueous solution due to their relatively high structural stability and low reactivity.[37] Therefore, this synthetic route also shows the potential for effectively functionalizing larger diameter SWCNTs and provides opportunities for fundamental studies and practical applications of OCCs in large diameter nanotube hosts.

DOI: 10.1021/acsnano.9b04087
ACS Nano 2019, 13, 8417−8424

CONCLUSIONS

We show that large-scale synthesis of organic color center-tailored SWCNTs can be achieved by simply mixing SWCNTs, $NaNO_2$, and an aniline derivative in chlorosulfonic acid and then introducing the mixture into water. Compared with existing OCC chemistries, our one-pot reaction features significant advantages, including that (1) the reaction occurs efficiently even at ultrahigh concentrations (>4000 μg/mL), making it readily scalable to synthesize large quantities of OCC-SWCNTs; (2) no surfactants or polymers are required to disperse the SWCNTs, thus the nanotube surfaces are "bare", free from molecular coating, and completely accessible for OCC implantation; (3) the reaction completes in seconds (*versus* days for aqueous diazonium salt reactions[1]); and (4) distinct from existing methods that require surfactant dispersion and work only for certain surfactants,[38,39] our method produces neat OCC-SWCNTs that can be directly encapsulated by specialized molecules/polymers that are required for subsequent applications (*e.g.*, chiral purification of OCC-SWCNTs). This facile, efficient, and scalable method has thus made large quantities of OCC-SWCNTs synthetically accessible for a broad range of applications in imaging,[40,41] sensing,[42,43] and quantum information processing.[44,45]

METHODS

Synthesis of OCC-SWCNTs. Raw SWCNT materials, including CoMoCat SG65i (Sigma-Aldrich) and HiPco (Rice University, batch number 194.3), were used for this large-scale preparation process. The SWCNTs were dissolved in chlorosulfonic acid (Sigma-Aldrich, 99%) at a concentration ranging from ~4 mg/mL with magnetic stirring, followed by the addition of an aniline derivative at different mole ratios relative to the SWCNT carbon and equimolar amounts of sodium nitrite (Sigma-Aldrich, ≥97.0%). We experimentally tested a wide variety of aniline derivatives for these experiments, including 3,5-dinitroaniline (Sigma-Aldrich, 97%), 4-nitroaniline (Sigma-Aldrich, ≥99.0%), 4-aminobenzoic acid (ReagentPlus, ≥99%), 2-fluoro-4-nitroaniline (Sigma-Aldrich, 95%), 4-amino-2-fluorobenzoic acid (Sigma-Aldrich, 97%), 4-amino-3-fluorobenzoic acid (Sigma-Aldrich, 97%), 4-amino-2,3,5,6-tetrafluorobenzoic acid (Sigma-Aldrich, 99%), 2-iodoaniline (Sigma-Aldrich, 98%), 4-chloroaniline (Sigma-Aldrich, 98%), and 4-aminophenol (Sigma-Aldrich, ≥98%). The SWCNT-superacid mixture was then added drop-by-drop into nanopure water with vigorous stirring by a Teflon-coated magnetic stir bar. (***Safety Note**: the neutralization process is aggressive; a significant amount of heat and acidic smog can be generated. Personal protective equipment, including goggles/facial masks, lab coats, and acid-resistant gloves, is necessary. The neutralization needs to be performed in a fume hood*). The resulting OCC-SWCNTs instantly precipitate out from the solution. The precipitates were then filtered on an AAO filtration membrane with pore size of 0.02 μm (Whatman Anodisc inorganic filter membrane), thoroughly rinsed with nanopure water, and then dried in a vacuum oven. By weighing the starting raw nanotubes and the synthesized OCC-SWCNTs we can estimate that the yield is approximately 97%. We note this yield does not consider the added weight due to the OCCs (which should be negligible) and the heterogeneity (in terms of the different functionalization degree on the individual nanotube level) in the synthesized OCC-SWCNTs.

Spectroscopic Characterization. The OCC-SWCNTs were stabilized by 2% (w/v) DOC, SDS, and CTAB in D_2O and 2% (w/v) PFO-BPy in toluene for PL measurements. The OCC-SWCNTs were dispersed in 2% (w/v) DOC-D_2O by tip ultrasonication with a power of 33 W and at 10 °C for 1 h, followed by centrifugation at 16 400 rpm for 1 h (Eppendorf centrifuge 5810R) to remove undissolved bundles. The PL spectra and excitation−emission maps of the SWCNT solutions were collected using a HORIBA Jobin Yvon NanoLog spectrofluorometer, with a 450 W xenon arc lamp and a liquid-N_2 cooled InGaAs array. UV−vis−NIR absorption spectra were acquired through a PerkinElmer Lambda 1050 spectrophotometer equipped with a broad InGaAs detector. Raman spectroscopy measurements were performed on a HORIBA Jobin Yvon LabRAM Raman microscope, and the spectrum of each sample was the average data for three different regions.

Hyperspectral Imaging. The OCC-SWCNTs were deposited on an imaging substrate by drop casting 10 μL of the OCC-SWCNT solution (2% (w/v) DOC-D_2O) and immediately blowing dry with N_2. The imaging substrate consisted of a thin, thermally deposited layer of gold (60 nm Au with a 5 nm thick Ti adhesion layer; Metra Thermal Evaporator) on a silicon wafer to improve the photon collection efficiency. A 50 nm thick polystyrene layer was spin coated on top of the Au to prevent fluorescence quenching. The hyperspectral imaging of the deposited OCC-SWCNTs was then performed on a custom-built shortwave IR imaging system that allows the acquisition of PL spectra from all pixels in the camera frame simultaneously.[23] The OCC-SWCNTs were excited with a 730 nm continuous wave laser (Shanghai Dream Lasers Technology Co., Ltd.) at 64 W cm^{-2}. The resulting fluorescence signal was collected by a 100× objective (LCPLN100XIR, numerical aperture (NA) = 0.85, Olympus) before sending the signal to a volume Bragg grating which was placed in front of the detector in the light path. The detector for the fluorescent signal was a Cougar-640 imaging camera (Xenics, Leuven, Belgium) with an InGaAs focal plane array with 640 × 512 pixels, cooled with liquid N_2 to −190 °C. An image stack was collected, one wavelength at a time, and reconstructed to provide the PL spectrum for each pixel over the entire field of view.

Sorting of OCC-SWCNTs. The ATPE method[33−35] was adapted and modified to separate OCC-SWCNTs with different chiralities. Briefly, 1 part of the OCC-SWCNT 2% (m/v) DOC solution was mixed with 0.3 parts of 20% (m/m) dextran (DX, MW 70 000 Da, TCI) and 0.3 parts of 50% polyethylene glycol (PEG, MW 6000 Da, Alfa Aesar) aqueous solution to yield ~0.2 parts of OCC-SWCNTs concentrated in the bottom DX-enriched phase after mild centrifugation at 4000*g* for 60 s. DOC surfactants were then gradually replaced by a sodium cholate (SC) and SDS cosurfactant system following the reported procedure so that the final concentration of SC and SDS were 0.9% (w/w) and 0.7% (w/w), respectively. The metallic/semiconducting SWCNT sorting process was then applied followed by diameter sorting until the desired chirality was enriched. We note that the OCC-(6,5)-SWCNT, OCC-(7,5)-SWCNT, OCC-(7,6)-SWCNT, and OCC-(8,4)-SWCNT were sorted from CoMoCAT SG65i, while the OCC-(8,7)-SWCNT and OCC-(12,1)-SWCNT were derived from the HiPco SWCNT starting material. The PEG and DX polymers were removed from the final semiconducting SWCNT-enriched solution by an ultrafiltration step using a centrifugal ultrafiltration nanotube (Amicon Ultra-15, PLHK Ultracel-PL membrane, 100 kDa), and the surfactants were exchanged to 2% (w/v) DOC in D_2O solution. Based on optical absorption measurements, the ATPE recovery yield for OCC-(6,5)-SWCNTs is estimated at ~58% after 5 sorting cycles. Note that the purity can be further improved with additional ATPE cycles at the cost of recovery yield.

Individually Dispersed, Long OCC-SWCNTs. A total of 10 mg of dried $C_6H_3(NO_2)_2$-OCC-tailored-SWCNT were fully dissolved in 50 mL of chlorosulfonic acid by magnetic stirring at 1200 rpm overnight. The OCC-SWCNT-superacid mixture was then added drop-by-drop into a 0.75 M NaOH and ~0.08% (w/v) DOC (Sigma-Aldrich, >97%) aqueous solution with vigorous stirring until the pH dropped to ~8. This neutralization is typically achieved by using 60 parts of 0.75 M NaOH-DOC for one part of OCC-SWCNT-superacid mixture. The solution was further stirred for 1 h followed by the addition of several drops of 1 M HCl aqueous solution to protonate the DOC molecules, causing them to coalesce into dark gray/black precipitates along with the SWCNTs. A 47 mm sized polyvinylidene fluoride filtration membrane was used to filter and collect the precipitates. The dark gray/black precipitates were then mixed with nanopure water and a few drops of 1 M NaOH to tune the pH to ~7 to 8. The slurry was stirred for 3 days, and the resulting

DOI: 10.1021/acsnano.9b04087
ACS Nano 2019, 13, 8417−8424

black solution was centrifuged at 16 400 rpm for 60 min (Eppendorf centrifuge 5810R) to remove undissolved SWCNT bundles.

Length Characterization of OCC-SWCNTs. Freshly cleaved mica (Ted Pella) was rinsed with 1 M $MgSO_4$ aqueous solution to positively charge the surface. A total of 50 μL of OCC-SWCNTs in 2% (w/v) DOC-D_2O was then drop cast onto the mica substrate and blown dry with N_2. All AFM images were recorded in tapping mode on a Cypher ES AFM (Asylum Research Corporation) with conical AFM probes backside-coated with gold (Tap300GD-G, with a force constant of 40 N/m and radius of curvature < 10 nm, BudgetSensors). All the images were acquired with a 30-μm piezoelectric stack scanner at a pixel resolution of 512 × 512 and analyzed using the Gwyddion software (version 2.53). In total 163 OCC-SWCNTs were analyzed for the average length characterization.

ASSOCIATED CONTENT

Supporting Information

The Supporting Information is available free of charge on the ACS Publications website at DOI: 10.1021/acsnano.9b04087.

Additional PL spectra and excitation−emission maps, UV−vis−NIR absorption spectra, and AFM and hyperspectral PL images (PDF)

AUTHOR INFORMATION

Corresponding Author

*(Y.H.W.) E-mail: yhw@umd.edu.

ORCID

Hong-Bin Luo: 0000-0002-2225-7072

Haoran Qu: 0000-0003-4536-6703

Xiaoming Ren: 0000-0003-0848-6503

YuHuang Wang: 0000-0002-5664-1849

Author Contributions

‖(H.-B.L. and P.W.) These authors contributed equally to this work.

Notes

The authors declare the following competing financial interest(s): Y.H.W., H.L., and P.W. are inventors on a pending U.S. patent application related to this work.

ACKNOWLEDGMENTS

This work is partially supported by NSF (Grant No. PHY-1839165). H.B.L. gratefully acknowledges the support provided by the China Scholarships Council (CSC No. 201708320366) during his visit to the University of Maryland. P.W. gratefully acknowledges the Millard and Lee Alexander Fellowship from the University of Maryland. AFM measurements were performed using a shared system supported by the NSF MRI program (CHE1626288).

REFERENCES

(1) Piao, Y.; Meany, B.; Powell, L. R.; Valley, N.; Kwon, H.; Schatz, G. C.; Wang, Y. Brightening of Carbon Nanotube Photoluminescence through the Incorporation of sp^3 Defects. *Nat. Chem.* **2013**, *5*, 840−845.

(2) Brozena, A. H.; Kim, M.; Powell, L. R.; Wang, Y. Controlling the Optical Properties of Carbon Nanotubes with Organic Color-Center Quantum Defects. *Nat. Rev. Chem.* **2019**, *3*, 375−392.

(3) Shiraki, T.; Uchimura, S.; Shiraishi, T.; Onitsuka, H.; Nakashima, N. Near Infrared Photoluminescence Modulation by Defect Site Design Using Aryl Isomers in Locally Functionalized Single-Walled Carbon Nanotubes. *Chem. Commun.* **2017**, *53*, 12544−12547.

(4) Wu, X.; Kim, M.; Kwon, H.; Wang, Y. Photochemical Creation of Fluorescent Quantum Defects in Semiconducting Carbon Nanotube Hosts. *Angew. Chem.* **2018**, *130*, 656−661.

(5) Maeda, Y.; Minami, S.; Takehana, Y.; Dang, J. S.; Aota, S.; Matsuda, K.; Miyauchi, Y.; Yamada, M.; Suzuki, M.; Zhao, R.-S.; Zhao, X.; Nagase, S. Tuning of the Photoluminescence and Up-Conversion Photoluminescence Properties of Single-Walled Carbon Nanotubes by Chemical Functionalization. *Nanoscale* **2016**, *8*, 16916−16921.

(6) Shiraki, T.; Onitsuka, H.; Shiraishi, T.; Nakashima, N. Near Infrared Photoluminescence Modulation of Single-Walled Carbon Nanotubes Based on a Molecular Recognition Approach. *Chem. Commun.* **2016**, *52*, 12972−12975.

(7) Kwon, H.; Furmanchuk, A.; Kim, M.; Meany, B.; Guo, Y.; Schatz, G. C.; Wang, Y. Molecularly Tunable Fluorescent Quantum Defects. *J. Am. Chem. Soc.* **2016**, *138*, 6878−6885.

(8) He, X.; Hartmann, N. F.; Ma, X.; Kim, Y.; Ihly, R.; Blackburn, J. L.; Gao, W.; Kono, J.; Yomogida, Y.; Hirano, A.; Tanaka, T.; Kataura, H.; Htoon, H.; Doorn, S. K. Tunable Room-Temperature Single-Photon Emission at Telecom Wavelengths from sp^3 Defects in Carbon Nanotubes. *Nat. Photonics* **2017**, *11*, 577−582.

(9) Kim, M.; Wu, X.; Ao, G.; He, X.; Kwon, H.; Hartmann, N. F.; Zheng, M.; Doorn, S. K.; Wang, Y. Mapping Structure-Property Relationships of Organic Color Centers. *Chem.* **2018**, *4*, 2180−2191.

(10) Saha, A.; Gifford, B. J.; He, X. W.; Ao, G. Y.; Zheng, M.; Kataura, H.; Htoon, H.; Kilina, S.; Tretiak, S.; Doorn, S. K. Narrowband Single-Photon Emission through Selective Aryl Functionalization of Zigzag Carbon Nanotubes. *Nat. Chem.* **2018**, *10*, 1089−1095.

(11) Gifford, B. J.; Kilina, S.; Htoon, H.; Doorn, S. K.; Tretiak, S. Exciton Localization and Optical Emission in Aryl-Functionalized Carbon Nanotubes. *J. Phys. Chem. C* **2018**, *122*, 1828−1838.

(12) Shirasaki, Y.; Supran, G. J.; Bawendi, M. G.; Bulović, V. Emergence of Colloidal Quantum-Dot Light-Emitting Technologies. *Nat. Photonics* **2013**, *7*, 13−23.

(13) Mandal, A. K.; Wu, X.; Ferreira, J. S.; Kim, M.; Powell, L. R.; Kwon, H.; Groc, L.; Wang, Y.; Cognet, L. Fluorescent sp^3 Defect-Tailored Carbon Nanotubes Enable NIR-II Single Particle Imaging in Live Brain Slices at Ultra-Low Excitation Doses. bioRxiv, 2019. DOI: https://doi.org/10.1101/636860 (accessed May 15, 2019).

(14) Hong, G.; Diao, S.; Antaris, A. L.; Dai, H. Carbon Nanomaterials for Biological Imaging and Nanomedicinal Therapy. *Chem. Rev.* **2015**, *115*, 10816−10906.

(15) Kwon, H.; Kim, M.; Meany, B.; Piao, Y.; Powell, L. R.; Wang, Y. Optical Probing of Local pH and Temperature in Complex Fluids with Covalently Functionalized, Semiconducting Carbon Nanotubes. *J. Phys. Chem. C* **2015**, *119*, 3733−3739.

(16) Yildirimer, L.; Thanh, N. T. K.; Loizidou, M.; Seifalian, A. M. Toxicology and Clinical Potential of Nanoparticles. *Nano Today* **2011**, *6*, 585−607.

(17) Kwon, H. J.; Shin, K.; Soh, M.; Chang, H.; Kim, J.; Lee, J.; Ko, G.; Kim, B. H.; Kim, D.; Hyeon, T. Large-Scale Synthesis and Medical Applications of Uniform-Sized Metal Oxide Nanoparticles. *Adv. Mater.* **2018**, *30*, 1704290.

(18) Powell, L. R.; Piao, Y.; Ng, A. L.; Wang, Y. Channeling Excitons to Emissive Defect Sites in Carbon Nanotube Semiconductors beyond the Dilute Regime. *J. Phys. Chem. Lett.* **2018**, *9*, 2803−2807.

(19) Hartmann, N. F.; Yalcin, S. E.; Adamska, L.; Hároz, E. H.; Ma, X.; Tretiak, S.; Htoon, H.; Doorn, S. K. Photoluminescence Imaging of Solitary Dopant Sites in Covalently Doped Single-wall Carbon Nanotubes. *Nanoscale* **2015**, *7*, 20521−20530.

(20) Haggenmueller, R.; Rahatekar, S. S.; Fagan, J. A.; Chun, J.; Becker, M. L.; Naik, R. R.; Krauss, T.; Carlson, L.; Kadla, J.; Trulove, P.; Fox, D.; DeLong, H.; Fang, Z.; Kelley, S. O.; Gilman, J. W. Comparison of the Quality of Aqueous Dispersions of Single Wall Carbon Nanotubes Using Surfactants and Biomolecules. *Langmuir* **2008**, *24*, 5070−5078.

(21) Wenseleers, W.; Vlasov, I. I.; Goovaerts, E.; Obraztsova, E. D.; Lobach, A. S.; Bouwen, A. Efficient Isolation and Solubilization of Pristine Single-Walled Nanotubes in Bile Salt Micelles. *Adv. Funct. Mater.* **2004**, *14*, 1105−1112.

(22) Islam, M. F.; Rojas, E.; Bergey, D. M.; Johnson, A. T.; Yodh, A. G. High Weight Fraction Surfactant Solubilization of Single-Wall Carbon Nanotubes in Water. *Nano Lett.* **2003**, *3*, 269−273.
(23) Wu, X.; Kim, M.; Qu, H.; Wang, Y. Single-Defect Spectroscopy in the Shortwave Infrared. *Nat. Commun.* **2019**, *10*, 2672.
(24) Davis, V. A.; Parra-Vasquez, A. N.; Green, M. J.; Rai, P. K.; Behabtu, N.; Prieto, V.; Booker, R. D.; Schmidt, J.; Kesselman, E.; Zhou, W.; Fan, H.; Adams, W. W.; Hauge, R. H.; Fischer, J. E.; Cohen, Y.; Talmon, Y.; Smalley, R. E.; Pasquali, M. True Solutions of Single-Walled Carbon Nanotubes for Assembly into Macroscopic Materials. *Nat. Nanotechnol.* **2009**, *4*, 830−834.
(25) Wang, P.; Kim, M.; Peng, Z.; Sun, C. F.; Mok, J.; Lieberman, A.; Wang, Y. Superacid-Surfactant Exchange: Enabling Nondestructive Dispersion of Full-Length Carbon Nanotubes in Water. *ACS Nano* **2017**, *11*, 9231−9238.
(26) Wang, P.; Peng, Z.; Li, M.; Wang, Y. Stretchable Transparent Conductive Films from Long Carbon Nanotube Metals. *Small* **2018**, *14*, 1802625.
(27) Wang, P.; Barnes, B.; Wu, X.; Qu, H.; Zhang, C.; Shi, Y.; Headrick, R.; Pasquali, M.; Wang, Y. Self-Sorting of 10-μm-Long Single-Walled Carbon Nanotubes in Aqueous Solution. *Adv. Mater.* **2019**, 1901641.
(28) Nam, C. W.; Kang, S.; Kang, Y.; Kwak, M. K. Cell Growth Inhibition and Apoptosis by SDS-Solubilized Single-Walled Carbon Nanotubes in Normal Rat Kidney Epithelial Cells. *Arch. Pharmacal Res.* **2011**, *34*, 661−669.
(29) Welsher, K.; Liu, Z.; Sherlock, S. P.; Robinson, J. T.; Chen, Z.; Daranciang, D.; Dai, H. A Route to Brightly Fluorescent Carbon Nanotubes for Near-Infrared Imaging in Mice. *Nat. Nanotechnol.* **2009**, *4*, 773−780.
(30) He, X.; Gifford, B. J.; Hartmann, N. F.; Ihly, R.; Ma, X.; Kilina, S. V.; Luo, Y.; Shayan, K.; Strauf, S.; Blackburn, J. L.; Tretiak, S.; Doorn, S. K.; Htoon, H. Low-Temperature Single Carbon Nanotube Spectroscopy of sp^3 Quantum Defects. *ACS Nano* **2017**, *11*, 10785−10796.
(31) Hersam, M. C. Progress Towards Monodisperse Single-Walled Carbon Nanotubes. *Nat. Nanotechnol.* **2008**, *3*, 387−394.
(32) Aharonovich, I.; Englund, D.; Toth, M. Solid-State Single-Photon Emitters. *Nat. Photonics* **2016**, *10*, 631−641.
(33) Gui, H.; Streit, J. K.; Fagan, J. A.; Hight Walker, A. R.; Zhou, C.; Zheng, M. Redox Sorting of Carbon Nanotubes. *Nano Lett.* **2015**, *15*, 1642−1646.
(34) Fagan, J. A.; Khripin, C. Y.; Silvera Batista, C. A.; Simpson, J. R.; Haroz, E. H.; Hight Walker, A. R.; Zheng, M. Isolation of Specific Small-Diameter Single-Wall Carbon Nanotube Species *via* Aqueous Two-Phase Extraction. *Adv. Mater.* **2014**, *26*, 2800−2804.
(35) Khripin, C. Y.; Fagan, J. A.; Zheng, M. Spontaneous Partition of Carbon Nanotubes in Polymer-Modified Aqueous Phases. *J. Am. Chem. Soc.* **2013**, *135*, 6822−6825.
(36) Capaz, R. B.; Spataru, C. D.; Ismail-Beigi, S. I.; Louie, S. G. Diameter and Chirality Dependence of Exciton Properties in Carbon Nanotubes. *Phys. Rev. B: Condens. Matter Mater. Phys.* **2006**, *74*, 121401.
(37) Dyke, C. A.; Tour, J. M. Covalent Functionalization of Single-Walled Carbon Nanotubes for Materials Applications. *J. Phys. Chem. A* **2004**, *108*, 11151−11159.
(38) Shiraki, T.; Niidome, Y.; Toshimitsu, F.; Shiraishi, T.; Shiga, T.; Yu, B.; Fujigaya, T. Solvatochromism of Near Infrared Photoluminescence from Doped Sites of Locally Functionalized Single-Walled Carbon Nanotubes. *Chem. Commun.* **2019**, *55*, 3662−3665.
(39) Shiraki, T.; Shiga, T.; Shiraishi, T.; Onitsuka, H.; Nakashima, N.; Fujigaya, T. Multistep Wavelength Switching of Near-Infrared Photoluminescence Driven by Chemical Reactions at Local Doped Sites of Single-Walled Carbon Nanotubes. *Chem. - Eur. J.* **2018**, *24*, 19162−19165.
(40) Liu, Z.; Tabakman, S.; Welsher, K.; Dai, H. Carbon Nanotubes in Biology and Medicine: *In Vitro* and *in Vivo* Detection, Imaging and Drug Delivery. *Nano Res.* **2009**, *2*, 85−120.
(41) Robinson, J. T.; Hong, G.; Liang, Y.; Zhang, B.; Yaghi, O. K.; Dai, H. *In Vivo* Fluorescence Imaging in the Second NearInfrared Window with Long Circulating Carbon Nanotubes Capable of Ultrahigh Tumor Uptake. *J. Am. Chem. Soc.* **2012**, *134*, 10664−10669.
(42) Biju, V. Chemical Modifications and Bioconjugate Reactions of Nanomaterials for Sensing, Imaging, Drug Delivery and Therapy. *Chem. Soc. Rev.* **2014**, *43*, 744−764.
(43) Farrera, C.; Torres Andon, F. T.; Feliu, N. Carbon Nanotubes as Optical Sensors in Biomedicine. *ACS Nano* **2017**, *11*, 10637−10643.
(44) Högele, A.; Galland, C.; Winger, M.; Imamoglu, A. Photon Antibunching in the Photoluminescence Spectra of a Single Carbon Nanotube. *Phys. Rev. Lett.* **2008**, *100*, 217401.
(45) Jeantet, A.; Chassagneux, Y.; Raynaud, C.; Roussignol, Ph; Lauret, J. S.; Besga, B.; Esteve, J.; Reichel, J.; Voisin, C. Widely Tunable Single-Photon Source from a Carbon Nanotube in the Purcell Regime. *Phys. Rev. Lett.* **2016**, *116*, 247402.

DOI: 10.1021/acsnano.9b04087
ACS Nano 2019, 13, 8417−8424